

Relativistic mergers of compact binaries in clusters: The fingerprint of the spin

Patrick Brem¹*, Pau Amaro-Seoane¹ & Rainer Spurzem^{2,3,4}

¹Max Planck Institut für Gravitationsphysik (Albert-Einstein-Institut), D-14476 Potsdam, Germany

²National Astronomical Observatories of China, Chinese Academy of Sciences, 20A Datun Lu, Chaoyang District, 100012, Beijing, China

³Astronomisches Rechen-Institut, Mönchhofstraße 12-14, 69120, Zentrum für Astronomie, Universität Heidelberg, Germany

⁴Kavli Institute for Astronomy and Astrophysics, Peking University, China

10 June 2021

ABSTRACT

Dense stellar systems such as globular clusters and dense nuclear clusters are the breeding ground of sources of gravitational waves for the advanced detectors LIGO and Virgo. The stellar densities reached in these systems lead to the dynamical formation of binaries at a rate superior to what one can expect in regions of the galaxy with lower densities. Hence, these systems deserve a close study to estimate rates and parameter distribution. This is not an easy task, since the evolution of a dense stellar cluster involves the integration of N bodies with high resolution in time and space and including hard binaries and their encounters and, in the case of gravitational waves (GWs), one needs to take into account important relativistic corrections. In this work we present the first implementation of the effect of spin in mergers in a direct-summation code, NBODY6. We employ non-spinning post-Newtonian corrections to the Newtonian accelerations up to 3.5 post-Newtonian (PN) order as well as the spin-orbit coupling up to next-to-lowest order and the lowest order spin-spin coupling. We integrate spin precession and add a consistent treatment of mergers. We analyse the implementation by running a set of two-body experiments and then we run a set of 500 simulations of a stellar cluster with a velocity dispersion set to a high value to induce relativistic mergers to set a proving ground of the implementation. In spite of the large number of mergers in our tests, the application of the algorithm is robust. We find in particular the formation of a runaway BH whose spin decays with the mass it wins, independently of the initial value of the spins of the BHs. We compare the result with 500 Monte Carlo realisations of the scenario and confirm the evolution observed with our direct-summation integrator. More remarkably, the subset of compact objects that do not undergo many mergers, and hence represent a more realistic system, has a correlation between the final absolute spin and the initial choice for the initial distribution, which could provide us with information about the evolution of spins in dense clusters once the first detections have started.

Key words: black hole physics – gravitational waves – methods: N -body simulations.

1 INTRODUCTION

The field of GWs has reached a milestone in the last years with the build-up of an international network of GW interferometers which have achieved their design sensitivity. The ground-based detectors LIGO and Virgo are undergoing major technical upgrades that will increase the volume of the observable universe by a factor of a thousand, which is referred to as the “advanced” configuration¹.

Dense stellar systems such as globular clusters, galactic nuclei and, in particular, dense nuclear clusters, are the breeding ground of the sources that the advanced detectors can expect (see the recent updated review of Benacquista & Downing 2011 and also Downing et al. 2011). More remarkably, the event rate of stellar-mass black hole binaries, the loudest kind of source, will be likely *dominated by sources formed dynamically*, i.e. via stellar close interactions in these stellar systems (Banerjee et al. 2010; Miller & Lauburg 2009; Downing et al. 2010; Benacquista & Downing 2011).

The data that will be harvested from the advanced detectors will allow us to do GW astrophysics. The con-

* E-mail: Patrick.Brem@aei.mpg.de (PB)

¹ <http://www.ligo.caltech.edu/advLIGO/>,
<http://wwwcascina.virgo.infn.it/advirgo/>

struction of templates for matched filtering is crucial in the searches for compact binaries. There have been efforts to construct these templates by combining post-Newtonian calculations of the inspiral of the binary with numerical relativity simulations of the merger and ringdown. Two appealing approaches are the effective-one-body technique (Buonanno & Damour 1999; Buonanno et al. 2009) and the phenomenological hybrid waveform modelling (Ajith et al. 2007, 2009; Santamaría et al. 2010).

However, the search will be challenging for the simple reason that a gravitational wave has not been detected yet. Reliable estimates of the event rates for the different kinds of binaries and of the expected parameter distribution will possibly be crucial for a successful detection. On the other hand, once we have the data, we will be able to compare the observed rates and parameters with the predictions derived from different models and thus filter them. This will enlighten our understanding of the creation and evolution of compact binaries in dense stellar systems.

The most accurate simulations of dense stellar clusters that we can do nowadays are performed with the so-called “direct-summation” N -body algorithms. In particular, the family of integrators of Sverre Aarseth has been in development for many decades (von Hoerner 1960, 1963; Aarseth 1963). Aarseth’s NBODY6 includes both *KS regularisation* (where KS stands for Kustaanheimo-Stiefel) and *chain regularisation*: when particles are tightly bound or their separation becomes too small, the system is regularised (see Kustaanheimo & Stiefel 1965; Aarseth 2003) to avoid too small individual time steps and numerical errors. It also employs the Ahmad-Cohen neighbour scheme (Ahmad & Cohen 1973) and hierarchical, adaptive time steps. We can hence resolve and follow accurately individual orbits in the system. In this article we present the first modification of a direct-summation code, using NBODY6, that includes all non-spinning PN corrections up to 3.5PN order and all spin contributions up to 2.5PN order, including spin precession equations.

2 THE FORMALISM AND ITS IMPLEMENTATION

2.1 Correction of the accelerations

We modify the acceleration computation as described in the pioneering work of Kupi et al. (2006) (KAS06) to include relativistic corrections, which are based on the post-Newtonian (PN) formalism for the interaction between two bodies. We note that recently Aarseth (2012) included an approximate implementation for relativistic corrections in the new version of his code, NBODY7. The relative acceleration, in the center-of-mass form, including all PN corrections used in the code can be written in the following way:

$$\frac{d\vec{v}}{dt} = -\frac{Gm}{r^2}[(1+A)\vec{n} + B\vec{v}] + \vec{C}_{1.5,SO} + \vec{C}_{2,SS} + \vec{C}_{2.5,SO}, \quad (1)$$

where $\vec{v} = \vec{v}_1 - \vec{v}_2$ is the relative velocity vector, $m = m_1 + m_2$ the total mass, r the separation and $\vec{n} = \vec{r}/r$. A and B are coefficients that can be found in Blanchet & Iyer (2003). The spin terms \vec{C}_N , where N denotes the PN order, are taken

from (Faye et al. 2006) and (Tagoshi et al. 2001). SO stands for spin-orbit and SS for spin-spin coupling.

These corrections are valid for two *isolated* bodies and shall thus only be applied to the Newtonian acceleration in the case of strong, “relativistic” pair-interactions where the perturbation by third bodies is sufficiently small. Because of this, we deem it reasonable to restrict the implementation of PN terms to regularised KS pairs (see Kustaanheimo & Stiefel 1965; Aarseth 2003, for details). For this reason we also choose the center-of-mass formulation shown in Eq. 1 rather than the formulation in the general frame. These KS pairs are only formed when the interaction between two bodies becomes strong enough so that the pair has to be regularised. During the KS regularisation the relative motion of the companions is still far from relativistic. Hence, only a small, relativistic subset of all regularised KS pairs will need post-Newtonian corrections. In order to match the order of accuracy of the KS integration in the code, we compute both the acceleration as shown in Eq. 1 as well as the analytical time derivative.

To save computational costs we switch on the PN corrections only if one of the following two conditions is fulfilled:

$$\begin{aligned} v &> \beta c \\ v &> \frac{\beta}{5}c, \text{ and } \frac{g_{PN}}{g} > \gamma_{rel}, \end{aligned} \quad (2)$$

where the parameters β and γ are chosen empirically to be $\beta = 0.02$ and $\gamma = 0.01$ and g_{PN} and g are the PN acceleration and the Newtonian acceleration, respectively². Note that this treatment differs from Aarseth (2012), who chooses a staggered scheme to switch on first PN 2.5, and later PN1 or PN2. We always switch on the complete set if equation 2 is fulfilled in order to maintain a correct orbit integration under PN influence. The switch-on criterion for the PN terms does not depend on the Newtonian perturbation of the regularised pair. Thus we also apply PN corrections to binaries that are being influenced by a third body. However, we note that for strong perturbations, NBODY6 automatically breaks up the KS pair and uses a Chain regularization algorithm for more than two bodies, in which we do not include any PN treatment due to the complications that arise by having more than two dominant objects.

2.2 Spin Precession

In addition to the effects on the acceleration, the spin of compact objects undergoes precession in relativistic two-body interactions. This is also taken into account by integrating the spin precession equations

² In order to avoid confusion, we denote the acceleration with the letter g , the dimensionless spin parameter with a and the semi-major axis with ξ .

$$\frac{d\vec{S}}{dt} = \frac{1}{c^2}\vec{U}_{1,\text{SO}} + \frac{1}{c^3}\vec{U}_{1.5,\text{SS}} + \frac{1}{c^4}\vec{U}_{2,\text{SO}} \quad (3)$$

$$\frac{d\vec{\Sigma}}{dt} = \frac{1}{c^2}\vec{V}_{1,\text{SO}} + \frac{1}{c^3}\vec{V}_{1.5,\text{SS}} + \frac{1}{c^4}\vec{V}_{2,\text{SO}} \quad (4)$$

$$\vec{S} = \vec{S}_1 + \vec{S}_2 \quad (5)$$

$$\vec{\Sigma} = m \left(\frac{\vec{S}_2}{m_2} - \frac{\vec{S}_1}{m_1} \right). \quad (6)$$

\vec{S} and $\vec{\Sigma}$ describe the spin state of the pair. The individual terms for \vec{U}_N and \vec{V}_N , where N denotes the PN order, can be found in (Faye et al. 2006) and (Buonanno et al. 2003).

2.3 Relativistic mergers

Since relativistic binaries lose energy via the dissipative 2.5PN acceleration term, we need to consistently add a relativistic “merger recipe” in the standard version of the code. For the purposes of our study, we must address the following points:

- (i) The criterion for two bodies to be transformed into one
- (ii) A dynamically correct treatment of the “loss” of one object from the simulation
- (iii) Computation of the spin of the BH that is formed after coalescence from the spins and orbital angular momentum of the BHs that participated in the coalescence

Post-Newtonian theory can only be applied to the inspiral of the binary, but not to the actual merger and ringdown. We choose for up to 3.5PN order a cut-off distance of $5 R_S$, with $R_S = 2G(m_1 + m_2)/c^2$ the combined Schwarzschild radius (Yunes & Berti 2008). For any instantaneous separation below this value, the pair is merged into one body.

On the other hand, the newly formed compact object must have a mass and a velocity vector consistent with the conservation of linear momentum. Also, since we are treating spinning compact objects, all BHs must have an initial spin vector. As we will see ahead, in section 3, we use a fitting formula at the last integration step before merging the bodies, i.e. at a separation of $5 R_S$, to assign a new spin value to the merged system following the prescription of Rezzolla et al. (2008).

The work we present in this article should be envisaged as a first testing of the algorithm with a “stress test”: Our goal is the integration of a large number of relativistic mergers in a stellar cluster. We achieve this, as we will see later, by setting initially the cluster in a relativistic stage with an extremely large central velocity dispersion. In order to maximise the number of mergers, we neglect the recoil of coalescing pairs, since merging BHs with a very large recoiling velocity could leave the system. However, a priori it is straightforward to implement a recipe for the gravitational recoil by following a similar fitting formula as in, e.g. the work of Pollney et al. (2007); Lousto et al. (2010).

3 TESTING THE IMPLEMENTATION

In this section we test the implementation itself in a direct-summation code. We present tests with a two-body integra-

tor based on the same routines as NBODY6, but restricted to a simple, regularised two-body system. This is exactly the part of the modification in the integration that we aim at implementing in NBODY6, and hence is a perfect testing ground of our algorithm.

In order to do so, we will compare our simple integrations with theoretical approaches. In this regard, the formulae of Peters (1964) are useful for testing the orbital decay in the simple non-spinning case. For spinning pairs we will check the precession frequencies and conservation of the total angular momentum.

3.1 Non-spinning, merging relativistic binaries

In this section we compare the results of our approximation with the derivation of Peters (1964) of the evolution of the eccentricity and semi-major axis of a binary which is decaying via the emission of GWs. His derivations are based on Keplerian orbits and mimic the 2.5 dissipative term in the post-Newtonian expansion.

$$\begin{aligned} \left\langle \frac{d\xi}{dt} \right\rangle &= -\frac{64 G^3 m_1 m_2 (m_1 + m_2)}{5 c^5 \xi^3 (1 - e^2)^{7/2}} \left(1 + \frac{73}{24} e^2 + \frac{37}{96} e^4 \right) \\ \left\langle \frac{de}{dt} \right\rangle &= -\frac{304}{15} e \frac{G^3 m_1 m_2 (m_1 + m_2)}{c^5 \xi^4 (1 - e^2)^{5/2}} \left(1 + \frac{121}{304} e^2 \right) \end{aligned} \quad (7)$$

In the last equations ξ is the semi-major axis, e the eccentricity, t the time, m_1 and m_2 the mass of the first and second star in the binary, G is the gravitational constant and c the speed of light. In the case of a circular binary, as shown in Peters (1964), one can solve the differential equation for a binary with companion masses m_1 , m_2 and initial semi-major axis ξ_0 :

$$\xi(t) = (\xi_0^4 - 4\beta t)^{1/4} \quad (8)$$

where

$$\beta = \frac{64 G^3 m_1 m_2 (m_1 + m_2)}{5 c^5}. \quad (9)$$

This yields a decay time of $T_c(\xi_0) = \xi_0^4/(4\beta)$.

In the general case of eccentric binaries, one can integrate Eq. (7) numerically and compare the time evolution with the results of our simulations. Since Peters’ formula is only valid for the leading order of gravitational radiation, we “switch off” the terms 1PN, 2PN, 3PN and 3.5PN and only apply the 2.5PN correction. In figure (1) and (2) we show the time evolution of eccentricity and semi-major axis for a system with two BHs of masses $m_1 = 10 M_\odot$ and $m_2 = 1 M_\odot$. They agree very well up to the limit of validity of the post-Newtonian expansion.

The 2.5 term only takes into account energy and angular momentum loss due to GWs. The 1 and 2 PN terms are conservative, they conserve energy and angular momentum, and they are the main contribution to periapsis shift.

In figures (3) and (4) we show the time evolution for a binary in which we have taken into account the correcting terms 1PN, 2PN and 2.5PN. Even though the 1 and 2PN terms are conserving energy, the binary coalesces quicker than in the Peters approximation, because they change the orbital velocity and thus the 2.5PN term acts slightly stronger. The small rise in eccentricity very close to the

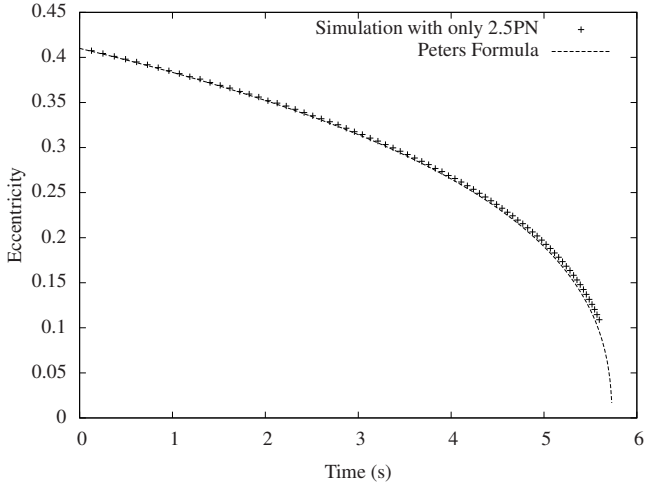


Figure 1. Comparison of the eccentricity evolution of the two-body integration and Peters' approximation.

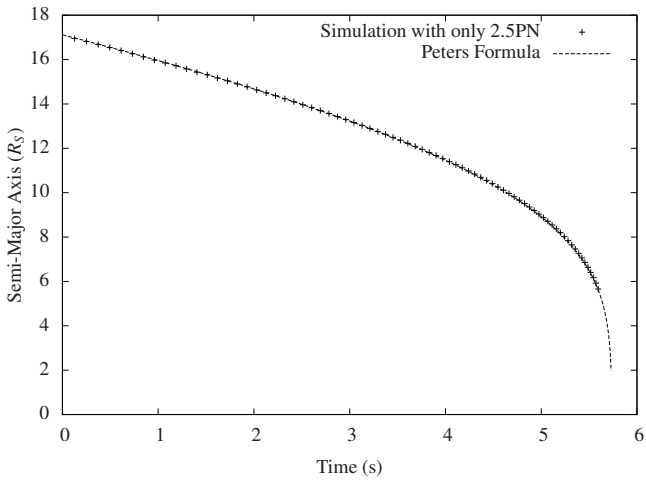


Figure 2. Comparison of the semi-major axis evolution of the two-body integration and Peters' approximation.

merger is a known effect of the PN expansion at the limits of its region of validity.

The contribution at 3PN and 3.5PN order are small compared to the leading order, but these terms cause the orbit to diverge when the binary enters the last few R_S ³. This is an important effect, since with PN terms up to order 2.5 one could in principle let the system evolve until an overlap of the Schwarzschild radii. When including 3PN and 3.5PN, on the other hand, this becomes impossible and in order to avoid unphysical, divergent behavior one has to abort the integration at larger separations. For this reason we choose the criterion $r = 5R_S$ where r is the instantaneous separation and R_S is the combined Schwarzschild radius.

³ Private communication with Seppo Mikkola and Cliff Will

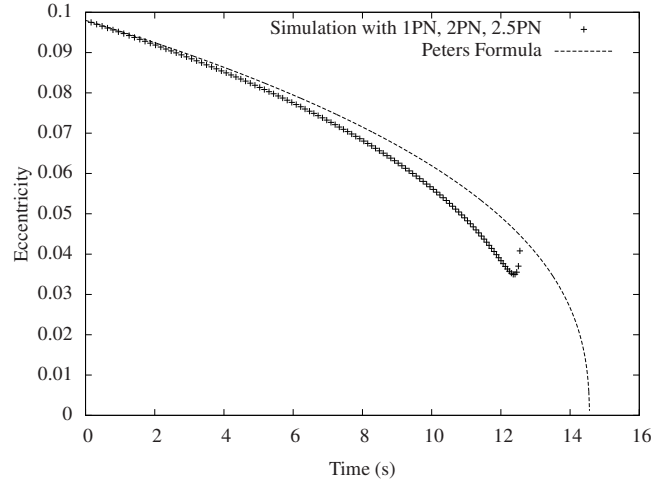


Figure 3. Comparison of the eccentricity evolution of the two-body integration with 1PN, 2PN and 2.5PN terms and Peters' approximation.

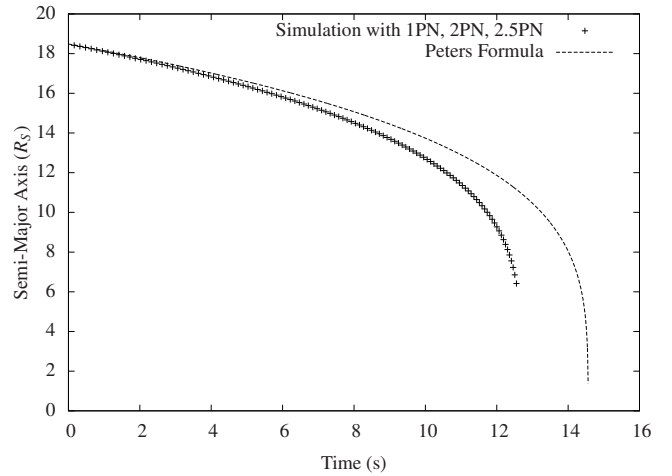


Figure 4. Comparison of the semi-major axis evolution of the two-body integration with 1PN, 2PN and 2.5PN terms and Peters' approximation.

3.2 Spinning binaries

3.2.1 Precession of angular momenta

In post-Newtonian theory, the Newtonian angular momentum $\vec{L}_N = \vec{x} \times \vec{p}$, with $\vec{p} = \vec{r} \times m \vec{v}$, is no longer conserved. In the case of non-spinning bodies, the direction of \vec{L}_N is conserved and only the modulus L_N is gradually radiated away during inspiral. However, in the case of spinning bodies this no longer holds (Kidder 1995). Nonetheless, as in electromagnetic theory, both the total spin vector \vec{S} and the angular momentum vector \vec{L} precess around the total angular momentum vector $\vec{J} = \vec{L} + \vec{S}$. The angular momentum vector we use differs from the usual Newtonian definition:

$$\vec{L} = \vec{L}_N + \vec{L}_{1PN} + \vec{L}_{SO} + \vec{L}_{2PN}. \quad (10)$$

With this definition, $\dot{\vec{J}} = 0$ up to 2PN order. The 2.5PN order, however, introduces radiation loss. Kidder (1995) esti-

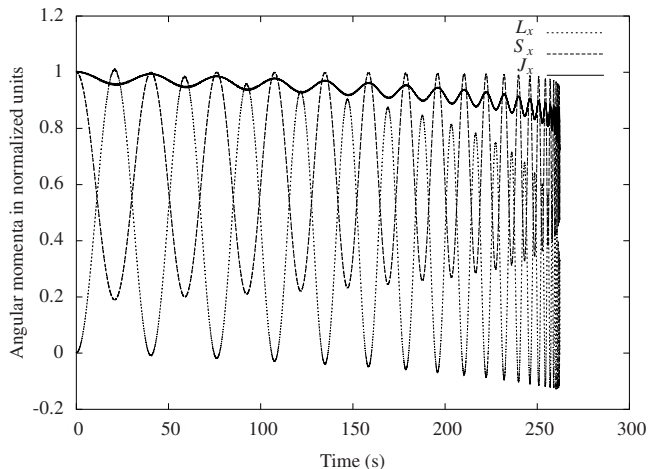


Figure 5. Angular momentum precession in the case of one spinning body. The total Newtonian angular momentum vector \vec{J}_N is approximately conserved.

mated the precession frequency to lowest order, i.e. $\vec{L} = \vec{L}_N$. In the case of a single spinning body with mass m_s in a system with total mass m , the precession frequency of both \vec{S} and \vec{L}_N is given by

$$\omega_p = \frac{G|\vec{J}|}{2c^2 r^3} \left(1 + 3 \frac{m}{m_s}\right). \quad (11)$$

As an example, let us consider a system of a maximally spinning black hole of mass $m_s = 10 M_\odot$ and a non-spinning companion of mass $m_2 = 1 M_\odot$. We set the system on a circular orbit in the x-y plane with radius 10^8 cm with the initial spin of m_s in x-direction. This gives a total initial angular momentum of

$$|\vec{J}| = \sqrt{L_z(t=0)^2 + S_{1,x}(t=0)^2} = 1.12 \times 10^{44} \frac{\text{kg m}^2}{\text{s}} \quad (12)$$

and thus a precession frequency of $\omega_p = 0.18$ Hz. We use non-spinning PN terms up to 3.5PN order and Spin-Orbit coupling up to next-to-leading order.

From figure (5) we can see that the approximate value for the period of the first precession cycle is (40.4 ± 0.4) s. This gives a value of $\omega_{p,\text{sim}} = 0.15$ Hz. The small difference comes from the fact that the calculation assumes the approximation $\vec{L} = \vec{L}_N$, and we are already in a very relativistic regime.

Even under the presence of spin-orbit precession, the direction of \vec{J}_N should be conserved. Fig. (6) shows the x-y-projection of \vec{J}_N and \vec{L}_N during an inspiral. One can see that the direction of \vec{J}_N is approximately constant but that the modulus shrinks due to gravitational radiation. During this process, \vec{L}_N precesses about this direction. One can also see the wobbles in the precession of the orbital plane given by \vec{L}_N , as described in the appendix of (Kidder 1995). This is due to the fact that in reality the corrected \vec{L} from Eq. (10) does the strict precession, which is not true for the Newtonian value \vec{L}_N , and hence leads \vec{L}_N to wobble about the conserved \vec{L} .

The check of \vec{J} conservation is a powerful way of testing

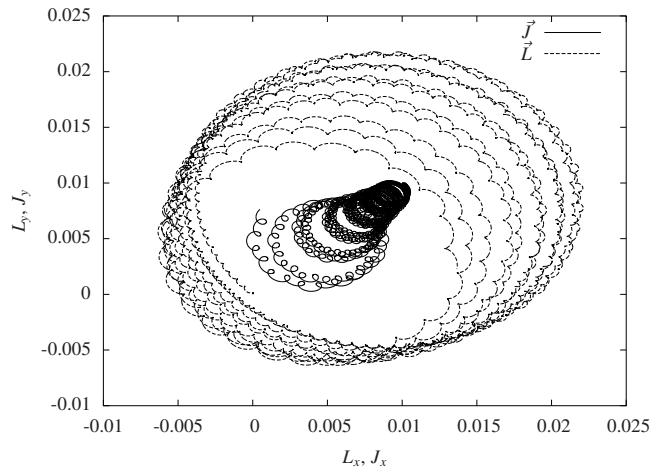


Figure 6. X-Y-projection of the angular momentum precession in the case of two maximally spinning bodies. Both \vec{J}_N and \vec{L}_N are gradually radiated away as \vec{L}_N precesses about \vec{J}_N .

the consistency of the approach to estimate the spin and angular momentum in the code.

3.3 Final spin approximation

In our code we are subject to the limitations of our post-Newtonian approach, which is not valid anymore when the relative speed becomes larger and larger, i.e. a few Schwarzschild radii before the merger. For this, we adopt the fitting formula of Rezzolla et al. (2008), derived from numerical simulations that address in full general relativity the last orbits of the binary, including merger and ringdown. We hence implement in the code the following formula for the modulus of the final spin (Rezzolla et al. 2008)

$$|\vec{a}_{\text{fin}}| = \frac{1}{(1+q)^2} [|\vec{a}_1|^2 + |\vec{a}_2|^2 q^4 + 2|\vec{a}_2||\vec{a}_1|q^2 \cos \alpha + 2(|\vec{a}_1| \cos \beta + |\vec{a}_2| q^2 \cos \gamma)|\vec{l}|q + |\vec{l}|^2 q^2]^{1/2}, \quad (13)$$

where $q = m_2/m_1$ is the mass ratio, \vec{a}_1 and \vec{a}_2 the dimensionless spin vectors and the angles are defined as

$$\begin{aligned} \cos \alpha &= \hat{a}_1 \cdot \hat{a}_2, \\ \cos \beta &= \hat{a}_1 \cdot \hat{l}, \\ \cos \gamma &= \hat{a}_2 \cdot \hat{l}. \end{aligned} \quad (14)$$

Therefore, so as to derive a value for the spin after merger, we need the individual spin vectors \vec{a}_1 , \vec{a}_2 and the orbital angular momentum (OAM) at an arbitrary point in time during inspiral. \vec{l} is a function of the OAM, given by

$$\begin{aligned} |\vec{l}| &= \frac{s_4}{(1+q^2)^2} (|\vec{a}_1|^2 + |\vec{a}_2|^2 q^4 + 2|\vec{a}_1||\vec{a}_2|q^2 \cos \alpha) \\ &+ \left(\frac{s_5 \eta + t_0 + 2}{1+q^2}\right) (|\vec{a}_1| \cos \beta + |\vec{a}_2| q^2 \cos \gamma) \\ &+ 2\sqrt{3} + t_2 \eta + t_3 \eta^2, \end{aligned} \quad (15)$$

where we use the fitting factors s_i , t_i given in Rezzolla et al. (2008). With Eq. (13) to (15) in hand, one can check whether

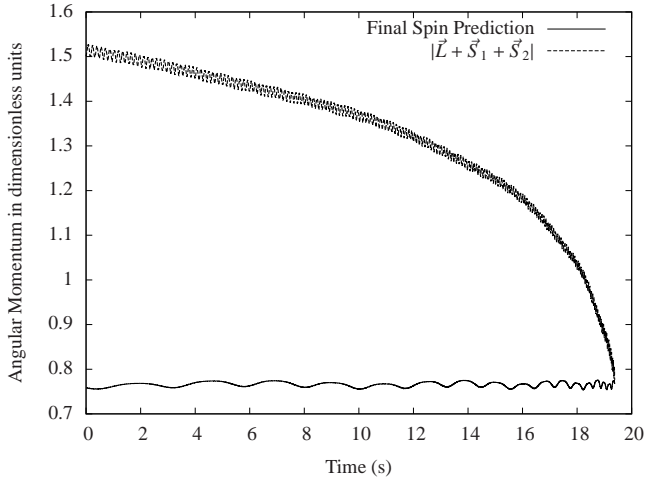


Figure 7. Comparison between the current final spin prediction and the actual total angular momentum of the binary system.

in the regime in which PN is valid, the simulation is consistent with this formula, in the sense that:

- (i) the total angular momentum must converge to the predicted absolute value
- (ii) the predicted final value should be independent of the time until coalescence.

Figure (7) shows the time evolution of both the predicted absolute value of the final spin at any given time during the inspiral and the actual total angular momentum. As one can see, for equal masses this gives a consistent value. \vec{J} is decreasing due to gravitational radiation until it reaches the prediction. At the latest times close to the merger, there will remain a small difference between \vec{J} and the predicted value due to the cut-off at $5R_S$ and due to other effects that are part of the numerical relativity simulations but not modelled in our PN integration.

3.4 Energy conservation

Since NBODY6 is a code to integrate Newtonian systems, it regularly checks whether the total energy of the system is conserved within some tolerance for numerical errors. In this work we have added relativistic terms in the PN approximation, so that this is no longer the case: (i) The dissipation, mainly by the 2.5PN term, causes a cumulative energy loss that has to be tracked and subtracted from the total energy. On the other hand, (ii) even the non-dissipative terms cause oscillations in the Newtonian energy, since only the modified expression,

$$E = E_{\text{Newt}} + E_{2.5\text{PN},\text{dis}} + E_{1\text{PN}} + E_{2\text{PN}} + E_{3\text{PN}} + \dots \quad (16)$$

is conserved at any given time. We thus calculate and subtract the corrections up to 3PN order from the total energy in order to construct the conserved quantity E . In this way we are able to verify energy conservation in the same way as it is usually done in purely Newtonian codes. This works well if the relativistic corrections are small. However, when $g_{\text{PN}}/g \approx 1$ the error induced by PN corrections will dominate and it becomes impossible to verify the correct integra-

tion of the system. In order to avoid this, one could decide an even larger distance threshold for merging two bodies into one or a criterion based on the relative strength of the PN corrections.

4 STELLAR-MASS BINARY MERGERS IN A CLUSTER: SOURCES OF GWS FOR GROUND-BASED DETECTORS

It is well-established that most galaxies should harbour a massive black hole in their centre, with a mass of some $10^{6-9}M_{\odot}$ (see e.g. Ferrarese & Ford 2005; Ferrarese et al. 2001; Kormendy & Gebhardt 2001). The densities observed may even exceed the core density of globular clusters by a factor hundred, and hence achieve about $10^7 - 10^8 M_{\odot} \text{pc}^{-3}$. Mass segregation creates a flow of compact objects towards the centre of the system (Lee 1987; Miralda-Escudé & Gould 2000; Khalisi et al. 2007; Preto & Amaro-Seoane 2010; Amaro-Seoane & Preto 2011), and may build up a cluster which could reproduce the effect of an MBH. Indeed, this has been used as an alternative to explain phenomena related to cluster evolution, like G1 and M15 (Banerjee & Kroupa 2011; Gebhardt et al. 2002; Baumgardt et al. 2003a,b; van der Marel et al. 2002). Nonetheless, for a globular cluster, compact objects such as stellar black holes are very likely expelled via three body interactions (Phinney & Sigurdsson 1991; Kulkarni et al. 1993; Sigurdsson & Hernquist 1993; Portegies Zwart & McMillan 2000). Lee (1995) proved that for $\sigma \gtrsim 300 \text{ km/s}$ the merger induced by gravity loss in clusters with two components is shorter than the required timescale for a third star to interact with a binary, so that clusters with higher velocity dispersions will not run into that problem. In this section we will test the robustness of our code by running simulations of dense stellar clusters with a very high velocity dispersion to trigger a large number of relativistic coalescences.

4.1 Initial conditions

To run a stress test on our implementation, we will consider that the clusters are represented by an isotropic Plummer sphere containing $N = 1,000$ stellar remnants of equal mass m . We use N -body units and choose a scaling according to KAS06 to trigger a significant amount of relativistic mergers to test the code. We set the central velocity dispersion to $\sigma_{\text{cen}} \approx 4,300 \text{ km s}^{-1}$, which is equivalent to fixing the ratio

$$\frac{\sigma_{\text{cen}}}{c} = \frac{1}{70}. \quad (17)$$

In other words, the speed of light “in code units” is $c = 70$. We consider therefore a cluster of compact objects with the same mass, spinning with a dimensionless spin parameter a and we consider three different initial spin setups for the compact objects at the time $T = 0$:

- Non-spinning ($a = 0$)
- Maximally spinning in the z-direction ($a = 1$)
- Random magnitude and orientation

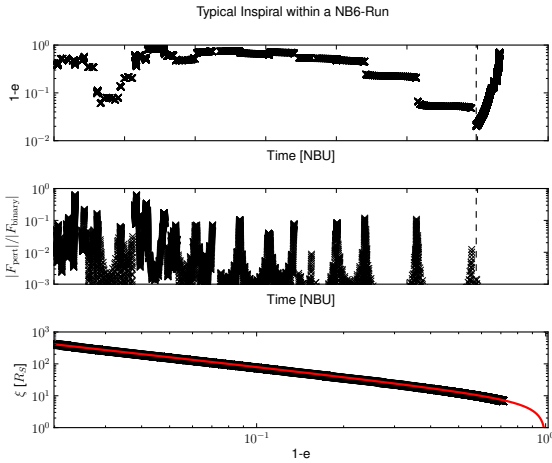


Figure 8. *Top panel:* Eccentricity evolution of one dynamically formed binary. First it is driven by Newtonian perturbations until the eccentricity reaches a critical value, from which the rapid circularization sets in. The dashed line marks the point from which we integrated Eq. (7) shown in the bottom panel. *Middle panel:* Perturbing force relative to the binary force. Strong changes in eccentricity are caused by strong Newtonian perturbations. *Bottom panel:* Inspiral as recorded in the simulation, compared to the analytical solution of Eq. (7) as the solid line.

4.2 Demonstration of a typical binary merger

We demonstrate here the evolution of a relativistic binary that has been formed dynamically within one of the non-spinning setups. Since we want to compare the decay to the approximation given by Eq. (7), only the dissipative 2.5PN term has been included. Figure 8 shows the evolution of the orbital elements and the Newtonian perturbation by third bodies relative to the binary force. The eccentricity evolves due to Newtonian perturbation until it reaches a critical value and the GW driven inspiral sets in. From this point, the solution of Eq. (7) is plotted for comparison. We note that in all plotted data points, the PN terms have been switched on and we thus confirm the robustness of our implementation under the presence of strong Newtonian perturbations.

4.3 Runaway growth

Because our system consists of very relativistic objects, almost any binary that forms and is regularized will undergo a quick merger due to the loss of orbital energy due to the dissipative 2.5PN term. Around the time of the core collapse, i.e. after some $\sim 15 T_{\text{rlx}}(T=0)$, with $T_{\text{rlx}}(T=0)$ the initial relaxation time of the cluster, a series of mergers leads to the formation of one particular BH in the system that rapidly grows in mass and becomes much more massive than the other objects. Therefore we say that the object runs away in mass. This is a consequence of the increase in cross section for GW capture. The time evolution of the mass of this runaway object is shown in figure 9. As we can see, after some $\sim 15 T_{\text{rlx}}(T=0)$, the runaway object has achieved $\sim 5\% M_{\text{cl}}(T=0)$, a value similar to the case studied in KAS06, their figure 1 around 450 time units.

An important issue that we need to address is the en-

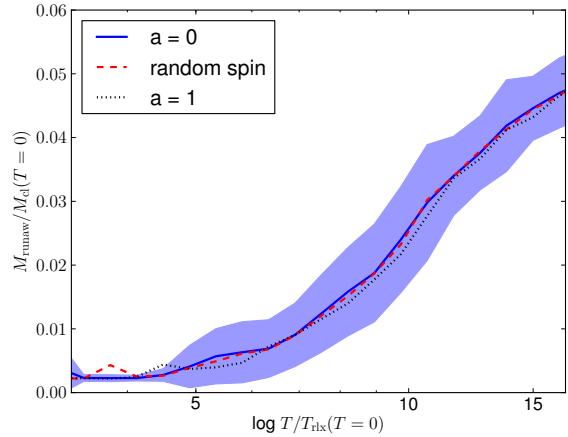


Figure 9. Mass of the runaway body, M_{runaway} , for each setup, averaged over 500 runs. $M_{\text{cl}}(T=0)$ is the total mass of the cluster at the time $T=0$ and $T_{\text{rlx}}(T=0)$ the initial relaxation time of the cluster. The shaded area shows the standard deviation for the $a=0$ case.

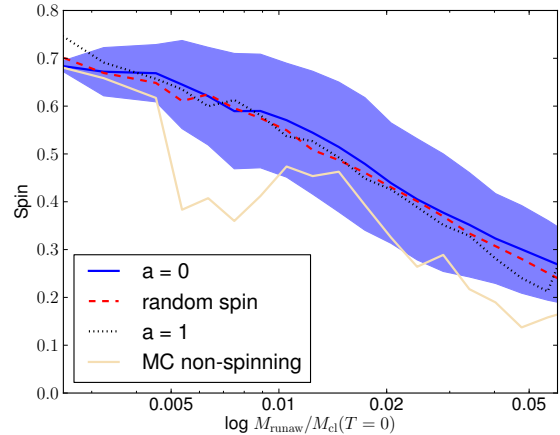


Figure 10. Spin of the runaway body in each simulation, averaged over 500 runs. The shaded area shows the standard deviation for the $a=0$ case. All initial spin setups lead to a similar evolution, except for the very first data point which is slightly higher for the maximally spinning initial conditions.

ergy conservation in the simulations. In figure 11 we show both the usual Newtonian energy and the corrected value, computed with Eq. (16) for a simulation with the same configuration as before but with $N=2000$ bodies. The Newtonian energy error grows with every single merger due to the dissipative PN terms. The corrected value for the energy conservation in our approach fluctuates significantly less and stays below 1%. The absolute value of the error depends on the nature of the merger: Head-on collisions dissipate the lowest amount of energy, while gradual inspirals lose the maximum amount before merger. The significant jump at $T=183$ corresponds to a binary which has spent a very long inspiral time due to a low eccentricity and a high initial separation. This causes rather high errors in the numerical integration of the dissipated energy at 2.5PN order

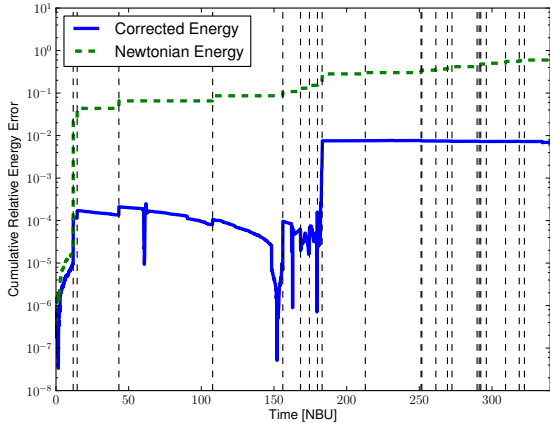


Figure 11. Cumulative relative energy error in a typical simulation. In this case we have 22 mergers, indicated by the dashed vertical lines, which cause the Newtonian energy error to grow significantly. Our alternative method to check for energy conservation leads to smaller fluctuations.

and thus contributes most to the total error, while some of the other mergers only cause relative errors of $\approx 10^{-4}$.

The absolute energy error depends crucially on the cut-off radius at which we end the integration and merge two bodies into one, because this sets the highest velocity we have to deal with in the binary. In this run we chose $10 R_S$. For smaller values, even the corrected error grows to the order of the total energy of the system. We note that even with larger errors induced by the dissipative PN terms, the global behavior of the simulation is not affected by the particular choice of the merger radius. If one wants a powerful energy conservation check it is reasonable to choose larger cut-off radii.

In order to be able to make a statistical comparison between each of the 3 spin setups and the potential impact on the evolution of the runaway body, we perform 500 simulations for each initial spin setup and show the mass averaged over each time bin. We can see in figure 10 the evolution of the spin for all 3 cases against the accumulated mass of the runaway object. Its formation is approximately the same in all three different scenarios, and consistent with the results of KAS06. Nonetheless, the precise point in time where the onset of the runaway process takes place depends sensitively on the scaling. In any case, the choice for the initial distribution of spins is washed out and all three cases show a consistent evolution for the runaway body. We additionally perform 500 Monte Carlo realisations of the scenario where one object merges with non-spinning compact objects coming in at random angles using the same final spin prediction as in the N -body code, so that we can test the statistical study. We depict the Monte Carlo spin evolution in figure 10 and confirm that this evolution is consistent with our N -body analysis within some scattering.

4.4 Evolution of individual spins

We now focus on the compact objects that have experienced only a few mergers. While the evolution of the spin of the

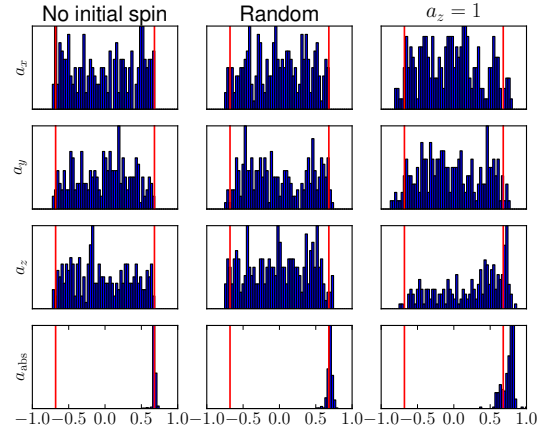


Figure 12. Spin distribution for those objects that have undergone at least one merger during the whole evolution of the cluster but not more than four. In the top panels we show three different initial choices for the spin of the BHs. From the left to the right we have first a cluster in which initially the BHs do not have spin, then a random value and in the last column a maximally spinning configuration around the z direction. From the top to the bottom panels we display the x -, y -, z - and absolute component of the spin ranging between -1 and 1 (a_x , a_y , a_z , a_{abs} shown on the left y -axis of the panels, respectively). The red lines depict the values -0.68 and +0.68.

runaway object quickly washes out any information regarding the initial spins, in the case of the other compact objects that do not undergo so many mergers, there is a dependence on the initial configuration even after core collapse. This is particularly interesting, since a trend in the evolution of the spin measurable with the advanced detectors would provide us with valuable information about the spin evolution of compact objects in clusters.

As mentioned in section 2.3, we did not include BH recoil. For any BH merger involving significantly spinning BHs, the recoil velocity can exceed the escape velocity and these merger products could thus leave the cluster. This means that the distribution presented here contains BHs that might no longer be part of the cluster itself.

In figure 12 we show the end distribution of spins for different initial configurations of the spin distribution for an otherwise identical system.

The configuration which initially had no spins is useful for comparison with the other systems. While the x -, y , and z -components individually show no clear trend, the absolute value is $a_{\text{abs}} = (0.69 \pm 0.02)$. If we move on to the second configuration, in which we initially assign all compact objects a spin but of random value, the final distribution is scattered around the same value, displayed with a red line in each of the panels at 0.68. In this case, the final value and standard deviation are $a_{\text{abs}} = 0.71 \pm 0.03$. Finally, if we give all compact objects initially a maximum value and set them in a preferred direction, which we arbitrarily choose to be the positive z -direction, the final distribution has a value of $a_{\text{abs}} = 0.76 \pm 0.08$.

In figure 13 we can also see this dependence. In the plot we display the time evolution of the total spin angular mo-

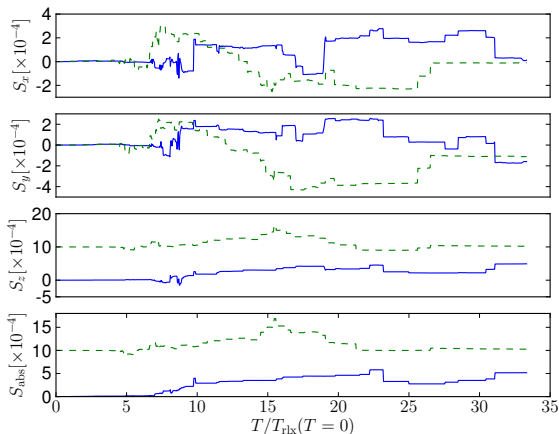


Figure 13. *Dashed green:* Total spin angular momentum for a cluster in which the remnants are initially maximally spinning in the z -direction. *Solid blue:* Total spin angular momentum for an initially non-spinning configuration.

mentum in the cluster, including the runaway object which carries most of the spin angular momentum. In the case of an initially non-spinning configuration, the spin builds up from orbital angular momentum and converges to a generic value in a similar way to what we showed in figure 12. We are limited in our analysis to derive the exact value to which the curve converges because of an accumulation of numerical errors.

5 CONCLUSIONS

In this work we have presented the first implementation of the effect of the spin for the treatment of relativistic mergers in a direct-summation N -body integrator. For that, we modify the calculation of the gravitational forces among particles using post-Newtonian up to 3.5 post-Newtonian (PN) order and the spin-orbit coupling up to next-to-lowest order and the lowest order spin-spin coupling.

We then check our implementations by running a series of tests to compare with results based on analytical derivations, for isolated two-body binaries and confirm the robustness of our approach. We also present a way to check for the correct integration of a system of N particles based on tracking the total energy, a usual test with this kind of integrators. Our method is valid provided the number of relativistic mergers in the system is low.

The final acid test of the implementation is to compare the global dynamical behaviour of a relatively large number of BHs with the new relativistic behaviour for binaries with well-known results based on similar approaches. More specifically, we run a similar test to that of KAS06 and obtain very similar results, which confirms the correct incorporation of the new terms in the code, since the initial spin distribution does not significantly change the global evolution of the system. This is so, because if two non-spinning, equal mass compact objects merge, the merger product will be spinning with $a \approx 0.68$ (Damour & Nagar 2007) in the direction of the angular momentum. Since in a Plummer

sphere there is no preferred direction in the distribution of the two-body angular momenta, this leads to a randomisation of the non-spinning distribution quickly. In the scenario of two maximum spins in the z -direction, i.e. individual spins of $S = Gm^2/c$ with equal masses m , the approximate angular momentum in the last stable orbit before merger is of the same order and thus also rotate the spins and similarly wash out the initially preferred direction.

For the larger subset of BHs that undergo a lower number of coalescences, which is more interesting since it is closer to what one could expect to see in a realistic cluster, we find that the evolution of the spin for consecutive mergers has a trend that oscillates around the value predicted by Damour & Nagar (2007), but with a scatter that is a fingerprint of the initial distribution of the isolated BHs, before they merged with any other in the system. This is particularly interesting, since this trend is what will determine the value of the spin that one can expect to see in globular clusters, and should be carefully assessed when developing the waveform banks to do the data analysis for the first detection.

Although the systems that we have explored in this work cannot be envisaged as representative examples of the grounds for which we expect the advanced detectors to observe relativistic mergers, the initial study of the behaviour of the code is a requirement before we proceed to more realistic systems, and has provided us with initial results which could play a crucial role in detection.

In particular, an immediate goal of our next research will be the study of the spin distribution and evolution in a dense stellar cluster with a realistic number of stars and including stellar evolution and primordial binaries, such as in (Downing et al. 2010, 2011), but with a more accurate direct N -body integrator. The history and distribution of black holes in a dense star cluster is also important for observing them in the electromagnetic windows, since it determines e.g. number and distribution of X-ray binaries and encounters between black holes and other compact objects such as neutron stars or white dwarfs.

Giersz et al. (2011) clearly show in their (non-relativistic) star cluster simulations using the Monte Carlo code that quite a few BHs and BH-BH binaries are formed and play a role for the dynamics of the central region. The presence of BHs may explain the size differences between red and blue globular clusters (Downing 2012) and affect the number of blue stragglers in a cluster (Hypki & Giersz 2013). These papers also discuss that relativistic recoils after merger not only important for the gravitational wave signal itself, but it is an important ingredient for correct modelling of globular clusters.

The kind of analysis we have presented in this work will soon have interesting applications, taking into account that the advanced ground-based detectors LIGO and VIRGO will have achieved their design sensitivity as soon as 2016-2017.

ACKNOWLEDGMENTS

We are indebted with Jonathan Downing and Peter Berczik for discussions. PB and PAS thank the National Astronomical Observatories of China, the Chinese Academy of Sciences and the Kavli Institute for Astronomy and Astrophysics in Beijing, for an extended visit. This work has

been supported by the Transregio 7 “Gravitational Wave Astronomy” financed by the Deutsche Forschungsgemeinschaft DFG (German Research Foundation). It has also been partially supported by the National Science Foundation under Grant No. PHYS-1066293 and the hospitality of the Aspen Center for Physics. RS acknowledges support by the Chinese Academy of Sciences Visiting Professorship for Senior International Scientists, Grant Number 2009S1-5 (The Silk Road Project). The simulations were run on the ATLAS cluster of the Albert-Einstein-Institute Hannover.

REFERENCES

- Aarseth S. J., 1963, *MNRAS*, 126, 223
—, 2003, *Gravitational N-Body Simulations*. ISBN 0521432723. Cambridge, UK: Cambridge University Press, November 2003.
—, 2012, *MNRAS*, 422, 841
Ahmad A., Cohen L., 1973, *Journal of Computational Physics*, 12, 389
Ajith P., Babak S., Chen Y., Hewitson M., Krishnan B., Sintes A. M., Whelan J. T., Brüggmann B., Diener P., Dorband N., Gonzalez J., Hannam M., Husa S., Pollney D., Rezzolla L., Santamaría L., Sperhake U., Thornburg J., 2009, *Ph. Rv. D*, 79, 129901
Ajith P., Babak S., Chen Y., Hewitson M., Krishnan B., Whelan J. T., Brüggmann B., Diener P., Gonzalez J., Hannam M., Husa S., Koppitz M., Pollney D., Rezzolla L., Santamaría L., Sintes A. M., Sperhake U., Thornburg J., 2007, *Classical and Quantum Gravity*, 24, 689
Amaro-Seoane P., Preto M., 2011, *Classical and Quantum Gravity*, 28, 094017
Banerjee S., Baumgardt H., Kroupa P., 2010, *MNRAS*, 402, 371
Banerjee S., Kroupa P., 2011, *ApJ Lett.*, 741, L12
Baumgardt H., Hut P., Makino J., McMillan S., Portegies Zwart S., 2003a, *ApJ Lett.*, 582, L21
Baumgardt H., Makino J., Hut P., McMillan S., Portegies Zwart S., 2003b, *ApJ Lett.*, 589, L25
Benacquista M. J., Downing J. M. B., 2011, *ArXiv e-prints*
Blanchet L., Iyer B. R., 2003, *Classical and Quantum Gravity*, 20, 755
Buonanno A., Chen Y., Vallisneri M., 2003, *prd*, 67, 104025
Buonanno A., Damour T., 1999, *Ph. Rv. D*, 59, 084006
Buonanno A., Pan Y., Pfeiffer H. P., Scheel M. A., Buchman L. T., Kidder L. E., 2009, *Phys. Rev. D*, 79, 124028
Damour T., Nagar A., 2007, *Phys. Rev. D*, 76, 044003
Downing J. M. B., 2012, *MNRAS*, 425, 2234
Downing J. M. B., Benacquista M. J., Giersz M., Spurzem R., 2010, *MNRAS*, 407, 1946
—, 2011, *MNRAS*, 416, 133
Faye G., Blanchet L., Buonanno A., 2006, *Ph. Rv. D.*, 74, 104033
Ferrarese L., Ford H., 2005, *Space Science Reviews*, 116, 523
Ferrarese L., Pogge R. W., Peterson B. M., Merritt D., Wandel A., Joseph C. L., 2001, *ApJ Lett.*, 555, L79
Gebhardt K., Rich R. M., Ho L. C., 2002, *ApJ Lett.*, 578, L41
Giersz M., Heggie D. C., Hurley J., Hypki A., 2011, *ArXiv e-prints*
Hypki A., Giersz M., 2013, *MNRAS*, 429, 1221
Khalisi E., Amaro-Seoane P., Spurzem R., 2007, *MNRAS*
Kidder L. E., 1995, *Phys. Rev. D*, 52, 821
Kormendy J., Gebhardt K., 2001, in *American Institute of Physics Conference Series*, Vol. 586, 20th Texas Symposium on relativistic astrophysics, Wheeler J. C., Martel H., eds., pp. 363–381
Kulkarni S. R., Hut P., McMillan S., 1993, *Nat*, 364, 421
Kupi G., Amaro-Seoane P., Spurzem R., 2006, *MNRAS*, L77+
Kustaanheimo P. E., Stiefel E. L., 1965, *J. Reine Angew. Math.*
Lee H. M., 1987, *ApJ*, 319, 801
—, 1995, *MNRAS*, 272, 605
Lousto C. O., Campanelli M., Zlochower Y., Nakano H., 2010, *Classical and Quantum Gravity*, 27, 114006
Miller M. C., Lauburg V. M., 2009, *ApJ*, 692, 917
Miralda-Escudé J., Gould A., 2000, *ApJ*, 545, 847
Peters P. C., 1964, *Physical Review*, 136, 1224
Phinney E. S., Sigurdsson S., 1991, *Nat*, 349, 220
Pollney D., Reisswig C., Rezzolla L., Szilágyi B., Ansorg M., Deris B., Diener P., Dorband E. N., Koppitz M., Nagar A., Schnetter E., 2007, *Phys. Rev. D*, 76, 124002
Portegies Zwart S. F., McMillan S. L. W., 2000, *ApJ Lett.*, 528, L17
Preto M., Amaro-Seoane P., 2010, *ApJ Lett.*, 708, L42
Rezzolla L., Barausse E., Dorband E. N., Pollney D., Reisswig C., Seiler J., Husa S., 2008, *Phy. Rev. D*, 78, 044002
Santamaría L., Ohme F., Ajith P., Brüggmann B., Dorband N., Hannam M., Husa S., Mösta P., Pollney D., Reisswig C., Robinson E. L., Seiler J., Krishnan B., 2010, *Phys Rev D*, 82, 064016
Sigurdsson S., Hernquist L., 1993, *Nat*, 364, 423
Tagoshi H., Ohashi A., Owen B. J., 2001, *Ph. Rv. D.*, 63, 044006
van der Marel R. P., Gerssen J., Guhathakurta P., Peterson R. C., Gebhardt K., 2002, *AJ*, 124, 3255
von Hoerner S., 1960, *Z. Astrophys.*, 50, 184
—, 1963, *Z. Astrophys.*, 57, 47
Yunes N., Berti E., 2008, *Ph. Rv. D*, 77, 124006